

# Reflection-Mode Bandstop Filters With Minimum Through-Line Length

Eric J. Naglich, *Member, IEEE*, and Andrew C. Guyette, *Senior Member, IEEE*

**Abstract**—This paper presents a technique that enables the design of high-order microwave bandstop filters with a total through-line length of significantly less than one quarter-wavelength at the filter center frequency. The total through-line length using this technique can be zero regardless of the filter order in theory, but it is limited in practice by the finite line length required to obtain a desired coupling magnitude between the through line and a resonator. A fifth-order quasi-elliptic reflection-mode bandstop filter design is shown with total through-line length of less than 1/15th of a wavelength in suspended-stripline technology. The measured response has a 42-MHz 30-dB bandwidth at a center frequency of 3 GHz and four reflection zeros. The bandstop filter design technique described in this paper shows great promise for reducing the size and weight of microwave bandstop filters.

**Index Terms**—Filter design, filters, filter synthesis, microwave filters, passive filters.

## I. INTRODUCTION

MICROWAVE bandstop filters are used to reflect or absorb unwanted signals in a microwave system. These unwanted signals can originate from co-site or externally generated interference, as well as nonlinear components under high-power excitation in the system. The traditional microwave bandstop filter is composed of resonators coupled to a through line with  $\lambda/4$  admittance inverters between each resonator [1]–[5]. The coupling-routing diagram of such a filter is shown in Fig. 1(a). This bandstop filter topology can produce a symmetric notch frequency response and meet a wide variety of practical specifications. However, when the traditional microwave bandstop filter topology is used for high-order filters, the total through-line length becomes long. A long through-line leads to increased circuit size, weight, and dispersive effects. In addition, the through-line lengths are difficult to tune in production environments yet have appreciable effects on the frequency response of the filter.

For the reasons mentioned above, techniques have been studied to reduce the total through-line length of microwave bandstop filters. In [6], filter designs with transmission line lengths between resonators that are less than  $\lambda/4$  were used in a design technique that produced wide upper passbands, which

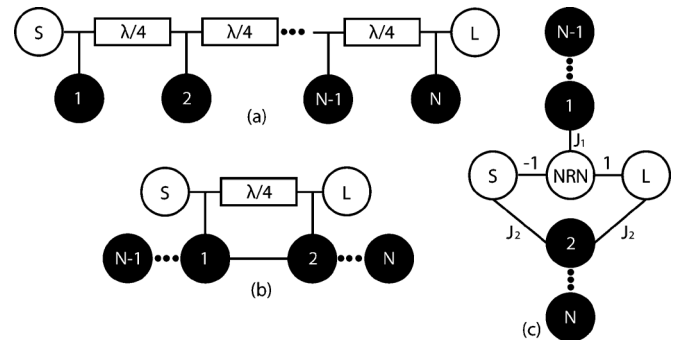


Fig. 1. Bandstop filter topologies. (a) Conventional bandstop filter with  $\lambda/4$  inverters between each resonator. (b) Cul-de-sac topology requiring only one  $\lambda/4$  length of line. (c) Bandstop topology used in this paper to realize bandstop filters with very short total through-line length. NRN value = 0.

are a desirable response trait in wide-bandwidth systems. The tradeoff when using the method in [6] is stopband asymmetry. In [7], a canonical transversal array network topology with source–load coupling is shown. With this network, it is possible to synthesize  $N$ th-order bandstop filters with  $N$  finite-frequency reflection zeros and a single quarter-wavelength section of through line. However, a transversal network becomes less practical as filter order is increased due to the large number of resonators that must be coupled to the input and output ports. More practical folded and cul-de-sac transformations of the transversal array shown in [7] are shown in [8] and [9]. The filters in these references have only a single quarter-wavelength section of through line regardless of their order and require only a single resonator coupled to both the input port and the output port. An example of the cul-de-sac topology is shown in Fig. 1(b). Bandstop filter design techniques using this and similar topologies to obtain high-order responses with only a single quarter-wavelength section of through line are well known and also called reflection-mode filters [10]–[15]. However, all previously demonstrated reflection-mode bandstop filters require at least one quarter-wavelength of through line.

This paper shows that the combination of the recently developed theory of bandstop filters with minimum through-line length [16] and the reflection-mode circuit topology can produce high-order bandstop filters with significantly less than  $\lambda/4$  total through-line length and symmetric responses. The coupling topology is shown in Fig. 1(c). Note that it is a standard reflection-mode topology [10]–[15]. However, when the relative signs and magnitudes of admittance inverters  $J_1$  and  $J_2$  are designed correctly to implement a minimum through-line-length bandstop filter [16], this topology can be implemented with a through-line length that is significantly

Manuscript received June 25, 2015; accepted August 02, 2015. This work was supported by the Defense Advanced Research Projects Agency (DARPA).

The authors are with Code 6851, U.S. Naval Research Laboratory, Washington, DC 20375 USA (e-mail: eric.naglich@nrl.navy.mil; andrew.guyette@nrl.navy.mil).

Color versions of one or more of the figures in this paper are available online at <http://ieeexplore.ieee.org>.

Digital Object Identifier 10.1109/TMTT.2015.2469660

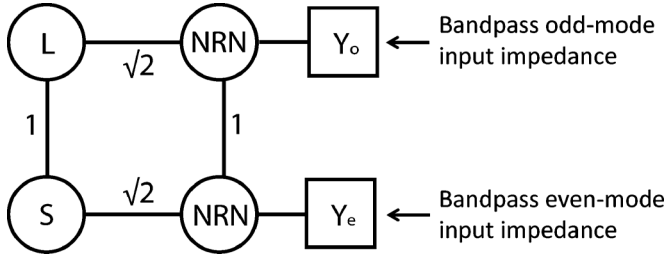


Fig. 2. Hybrid reflection-mode bandstop filter topology. NRN value = 0.

shorter than  $\lambda/4$ . The approach includes tradeoffs that involve the achievable upper passband width and maximum stopband attenuation when pushed to its limits, but the design space includes filter performance that is desirable for many practical applications. The proposed combination is expected to reduce the size and weight of future microwave bandstop filters.

## II. THEORY

### A. Reflection-Mode Bandstop Filters

A reflection-mode bandstop filter can be constructed by first designing a prototype bandpass filter with a reflection coefficient that is equivalent to the transmission coefficient of the desired bandstop filter [10]. Circuits that implement the even- and odd-mode impedances of the prototype bandpass filter are connected to two adjacent ports of a four-port hybrid circuit, as shown in Fig. 2. The remaining two ports of the hybrid circuit are used as source and load ports. The combined circuit retains the even-mode impedance of the prototype bandpass filter, but inverts the odd-mode impedance. When the odd-mode impedance of any linear network is inverted, the reflection coefficient becomes the transmission coefficient and vice-versa. Therefore, since the initial prototype network was a bandpass filter, a bandstop response is produced.

While reflection-mode bandstop filters have shorter through-line lengths than traditional inline bandstop filters, their ultimate stopband attenuation is limited by either the isolation of the hybrid circuit used or the minimum value of the reflection coefficient obtained in the prototype bandpass filter whose transmission poles are inverted by the hybrid circuit. Although it is possible in theory to design a prototype bandpass filter response with a very small passband reflection coefficient, it is very difficult in practice to fabricate a high-order bandpass filter with a passband impedance match to  $50 \Omega$  that is significantly better than  $-30$  dB. Therefore, the stopband attenuation of reflection-mode bandstop filters will also be limited to approximately 30 dB. In order to achieve higher amounts of stopband attenuation, reflection-mode filters can be cascaded. Although this increases total through-line length, it is often still significantly shorter than the through-line length of traditional inline topologies.

### B. Bandstop Filters With Minimum Through-Line Length

A conventional microwave bandstop filter design with  $\lambda/4$  inverters between each resonator assumes that the coupling structures between the through-line and the resonators all

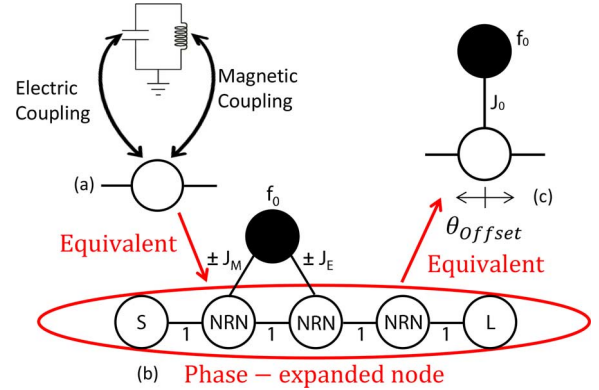


Fig. 3. Mixed coupling from a through line to a resonator. (a) Resonator coupled to node with both electric and magnetic coupling. (b) Phase-expanded node showing relative phase between electric and magnetic coupling to the node. (c) Representation of the node in (b) as a phase offset dependent on the signs and magnitudes of  $J_E$  and  $J_M$ . NRN values = 0.

implement coupling with either electric field, magnetic field, or the same relative mixture of electric and magnetic field. However, if mixed electric and magnetic field coupling is used and the relative field strengths are intelligently designed for each coupling structure, effective phase offsets can be produced between resonators along the through line [16], [17]. These phase offsets can be used to absorb some or all of the length of the  $\lambda/4$  inverters between resonators. This concept is shown in Fig. 3. In Fig. 3(a), a mixture of electric and magnetic coupling between a resonator and a node on a through-line is shown. Fig. 3(b) shows an equivalent circuit of Fig. 3(a) where the node has been expanded in phase to show the relative phase shift between magnetic ( $J_M$ ) and electric ( $J_E$ ) field coupling. The composite phase offset due to multiple types of coupling between a single node and a resonator can be reduced to the circuit in Fig. 3(c), where

$$J_0 = \sqrt{(J_E^2 + J_M^2)} \quad (1)$$

and

$$\theta_{offset} = \frac{1}{2} \text{Arg} \left( \frac{2J_E}{J_E - jJ_M} - 1 \right). \quad (2)$$

Reference [16] uses mixed electric and magnetic field coupling to resonators along a through line to implement (1) and (2) in a fourth-order minimum through-line-length bandstop filter design. Each resonator is coupled to the through line over a  $\lambda/8$  physical length of line and implements a  $\lambda/8$  electrical shift of the coupling reference plane between it and the next resonator,  $\theta_{offset}$ , through the use of appropriately designed mixed coupling to create a composite  $\lambda/4$  inverter between each resonator. A photograph of the filter in [16] can be seen in Fig. 4. The  $\lambda/8$  physical coupling section for each resonator is followed directly by the  $\lambda/8$  physical coupling section for the next resonator, so the entire length of the through line is coupled to a resonator.

While this technique enables an improvement over conventional designs that have a total through-line length of  $N * \lambda/4$ , where  $N$  is the order of the filter, the total through-line length,  $N * L_c$ , where  $L_c$  is the length of the coupling section between the through line and each resonator, can still be significant for high-order filters. The combination of reflection-mode

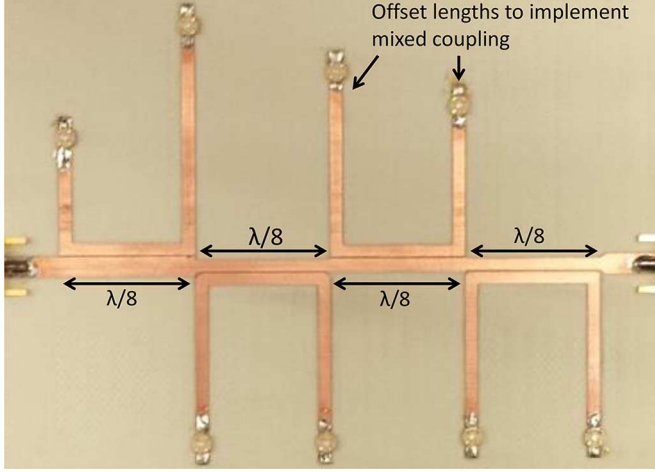


Fig. 4. Photograph of bandstop filter in [16].

circuit techniques and minimum through-line-length bandstop filter theory can produce bandstop filter designs with a total through-line length equal to only the length of a single coupling section,  $L_c$ , regardless of filter order. Therefore, the total through-line length becomes only a function of the desired coupling values and fabrication technology tolerances, not filter order, and it can be much shorter than  $\lambda/4$  for many filter specifications.

### C. Second-Order Example

In order to present the concept with readable and easier-to-follow equations, a second-order example design will be shown first. The goal of this section is to find the even- and odd-mode admittances of a prototype low-pass filter and then show that the reflection-mode topology can implement a prototype high-pass filter with a transmission coefficient equal to the reflection coefficient of the low-pass prototype and vice-versa. The high-pass prototype can be transformed to produce a bandstop response using standard circuit techniques [18]. A second-order 20-dB equi-ripple Chebyshev low-pass filter prototype will be used as the starting point. However, any low-pass prototype filter can be used for the design procedure. A coupling-routing diagram for the prototype low-pass filter is shown in Fig. 5(a). The red dashed line through the  $J_{12}$  admittance inverter is the symmetry plane used for even-odd mode analysis, and the even- and odd-mode subcircuits can also be seen in Fig. 5(a). For the even mode, the  $J_{12}$  admittance inverter becomes an open-circuited  $\lambda/8$  length of line with a characteristic admittance of  $J_{12}$ , and the even-mode input admittance of the prototype circuit is

$$Y_e = \frac{J_0^2}{p + jJ_{12}} \quad (3)$$

where  $j$  is the square root of  $-1$  and  $p$  is the frequency variable  $j\omega$ . For the odd mode, the  $J_{12}$  admittance inverter becomes a short-circuited  $\lambda/8$  length of line with a characteristic admittance of  $J_{12}$ , and the odd-mode input admittance of the prototype circuit is

$$Y_o = \frac{J_0^2}{p - jJ_{12}}. \quad (4)$$

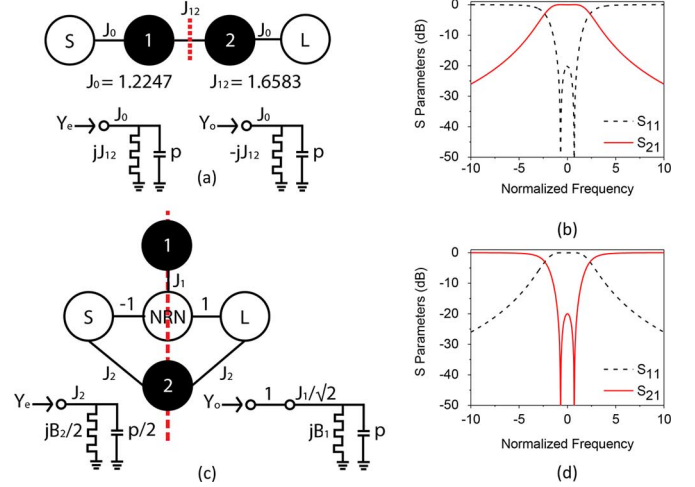


Fig. 5. Second-order coupling-routing diagrams and responses. (a) Second-order 20-dB equi-ripple Chebyshev low-pass prototype. (b) Response of prototype in (a). (c) Two-pole version of the reflection-mode topology. NRN value = 0. (d) Response of prototype in (c).

The reflection and transmission coefficients of the network can be found using the following equations:

$$S_{11} = \frac{1 - Y_e Y_o}{(1 + Y_e)(1 + Y_o)} \quad (5)$$

and

$$S_{21} = \frac{Y_o - Y_e}{(1 + Y_e)(1 + Y_o)}. \quad (6)$$

The normalized responses obtained from (5) and (6) are plotted in Fig. 5(b).

Fig. 5(c) shows the two-pole version of the reflection-mode topology in Fig. 1(c) with a red dashed line (in online version) that indicates the plane of symmetry for even-odd-mode analysis. It is important to note that the lower path through resonator 2 in Fig. 5(c) is symmetric about the dashed line, while the path through the non-resonating node (NRN) is antisymmetric about the dashed line due to the opposite signs of the unity-magnitude inverters. An antisymmetric path will have opposite terminations in even-odd-mode analysis relative to the symmetric case. For the even mode, the antisymmetric path is shorted to ground, and the even-mode input admittance of the prototype circuit is

$$Y_e = \frac{J_2^2}{\frac{1}{2}(p + jB_2)} \quad (7)$$

where  $B_2$  is a frequency-invariant susceptance that manifests as a shift of the center frequency of resonator 2.

For the odd mode, the lower path through resonator 2 is shorted to ground, and the odd mode input admittance of the prototype circuit is

$$Y_o = \frac{2(p + jB_1)}{J_1^2} \quad (8)$$

where  $B_1$  is a frequency-invariant susceptance that manifests as a shift of the center frequency of resonator 1. Comparing the input admittances in (3) and (4) to those in (7) and (8), it can be seen that the even-mode admittances have the same form. However, the forms of the odd-mode admittances are inverses

of each other. Therefore, the reflection-mode topology can produce a high-pass response with a transmission coefficient equal to the low-pass prototype's reflection coefficient if  $J_1$ ,  $J_2$ ,  $B_1$ , and  $B_2$  are designed properly. Setting (3) equal to (7) and (4) equal to the inverse of (8) and solving for the desired quantities yields

$$B_1 = -J_{12} \quad (9)$$

$$J_1 = \sqrt{2}J_0 \quad (10)$$

$$B_2 = J_{12} \quad (11)$$

$$J_2 = \frac{J_0}{\sqrt{2}}. \quad (12)$$

Plugging the values in (9)–(12) into (7) and (8) and plotting the reflection-mode circuit's S-parameters using (5) and (6) results in the plot shown in Fig. 5(d), which is a high-pass response and the inverse of the low-pass response shown in Fig. 5(b).

#### D. Fifth-Order Example

The coupling-routing diagram of a fifth-order bandpass filter is shown in Fig. 6(a). The filter was designed using Coupling Matrix Synthesis Software from Guided Wave Technology to have a center frequency of 3 GHz, a 30-dB equi-ripple return-loss bandwidth of 45 MHz, and transmission zeros at 2.92, 2.96, 3.04, and 3.08 GHz. The synthesized response of the filter can be seen in Fig. 6(c), and the normalized  $N + 2 \times N + 2$  coupling matrix [19] is shown in (13) at the bottom of this page. The topology in Fig. 6(a) was chosen because it is simple to analyze with even-odd-mode analysis. Note that due to the signs of  $J_{S1}$  and  $J_{S3}$ , the lower path is symmetric about the vertical line of symmetry through the middle of the circuit while the upper path is antisymmetric. Therefore, the lower path forms the even-mode circuit and the upper path forms the odd-mode circuit. Using the same even- and odd-mode analysis procedure shown in the second-order example, the even- and odd-mode admittances of the fifth-order bandpass filter can be found and set equal to the even- and odd-mode admittances of the fifth-order reflection-mode bandstop topology shown in Fig. 6(b). The response of this network can be seen in Fig. 6(d), and the normalized  $N + 2 \times N + 2$  coupling matrix is shown in (14) at the bottom of the following page. Note that  $J_{N1}$  is double the value of  $J_{S1}$ , but all other admittance inverter parameters are equal to the values in the bandpass prototype. The result is a 30-dB equi-ripple bandstop response with four reflection zeros. This response was used as a target specification to design and fabricate a suspended-stripline prototype circuit for verification.

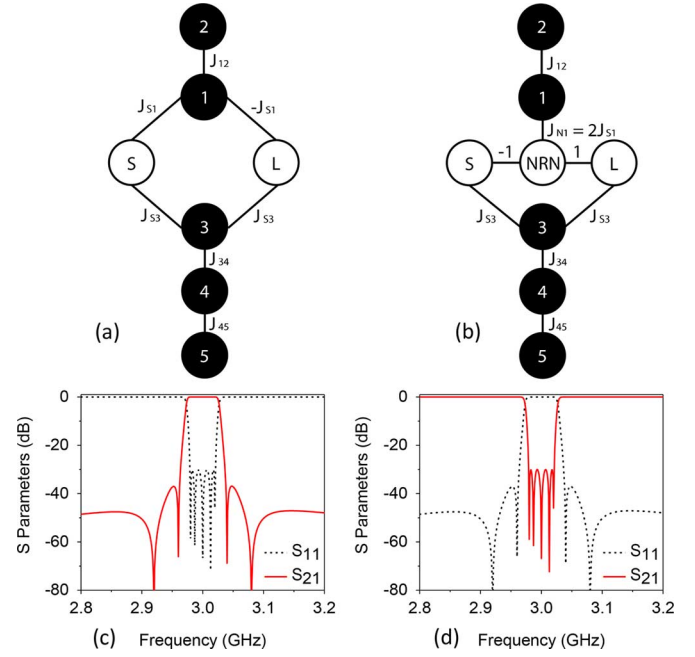


Fig. 6. Fifth-order topologies. (a) Fifth-order bandpass filter prototype. (b) Fifth-order reflection-mode bandstop topology. NRN value = 0. (c) Shifted and scaled frequency response of the bandpass prototype in (a). (d) Shifted and scaled frequency response of the bandstop prototype in (b).

### III. FIFTH-ORDER PROTOTYPE DESIGN AND FABRICATION

In Fig. 6(b), resonators 1 and 3 are coupled to the through line. This section of the topology is reproduced more generally in Fig. 7(a). The coupling-routing diagram in Fig. 7(a) can be implemented in suspended stripline as shown in Fig. 7(b), where a stripline resonator is coupled to the through line at an electric-field maximum above the through line and another stripline resonator is coupled to the through line at a magnetic-field maximum below the through line. The lateral center of both resonators align. In this topology, one  $J_M$  admittance inverter is implemented with the left half of the magnetically coupled section, and the other  $J_M$  admittance inverter is implemented with the right half of the magnetically coupled section. Since the path through the NRN has a total phase shift of  $0^\circ$  due to the two opposite-signed inverters, the couplings from both  $J_M$  admittance inverters are in phase and can be physically implemented as a single magnetic coupling structure. In most relevant suspended stripline resonator geometries, the minimum length of the coupling structure in Fig. 7(b) will be set by the length required to

$$\begin{bmatrix} 0 & 0.8484 & 0 & 0.8616 & 0 & 0 & 0 \\ 0.8484 & 0.0027 & 1.1754 & 0 & 0 & 0 & -0.8484 \\ 0 & 1.1754 & -0.0066 & 0 & 0 & 0 & 0 \\ 0.8616 & 0 & 0 & -0.0011 & 0.9435 & 0 & 0.8616 \\ 0 & 0 & 0 & 0.9435 & 0.0112 & 1.0790 & 0 \\ 0 & 0 & 0 & 0 & 1.0790 & -0.0128 & 0 \\ 0 & -0.8484 & 0 & 0.8616 & 0 & 0 & 0 \end{bmatrix} \quad (13)$$

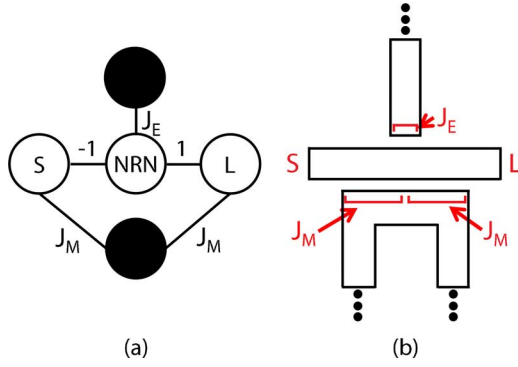


Fig. 7. Short through-line coupling section to first two resonators. (a) Coupling-routing diagram. NRN value = 0. (b) Physical implementation in suspended stripline.

obtain the desired magnitudes of the  $J_M$  admittance inverter parameters, which can be quite short for some filter specifications.

Sonnet and AWR Microwave Office software were used to design the fifth-order suspended stripline filter prototype. Initially, Sonnet was used to design resonators and coupling sections for a 3-GHz center frequency, 45-MHz 30-dB equi-ripple bandstop filter with response shape given by (14). Once the individual resonators approximately had the desired center frequencies and coupling values, a composite Sonnet simulation was created. The composite simulation has co-calibrated ports inserted into the resonators and coupling sections so that sNp files, where N is the number of ports in the simulation file, could be exported to AWR Microwave Office and tuned to account for changes in values after combination of the circuit elements. The lengths of the resonators and coupling sections were slightly tuned in AWR Microwave Office and then updated in Sonnet iteratively until the tuning lengths in AWR Microwave Office were approximately zero. Finally, tuning capacitor ports were included into the Sonnet simulation to enable post-fabrication tuning of the resonator center frequencies and coupling values. The final Sonnet layout with critical dimensions listed can be seen in Fig. 8. Both conductor layers of a 0.127-mm-thick Rogers 6202 circuit board ( $\epsilon_r = 2.94$ ,  $\tan(\delta) = 0.0015@10$  GHz) were used so that the through line and resonators could overlap for increased coupling. 1.5 mm of air dielectric was used between the circuit board and aluminum ground planes above and below the circuit board in the simulation.

Half-wavelength resonators were chosen for resonators 2–5, and a quarter-wavelength resonator that is shorted to ground on one side was chosen for resonator 1. Note that the resonators are

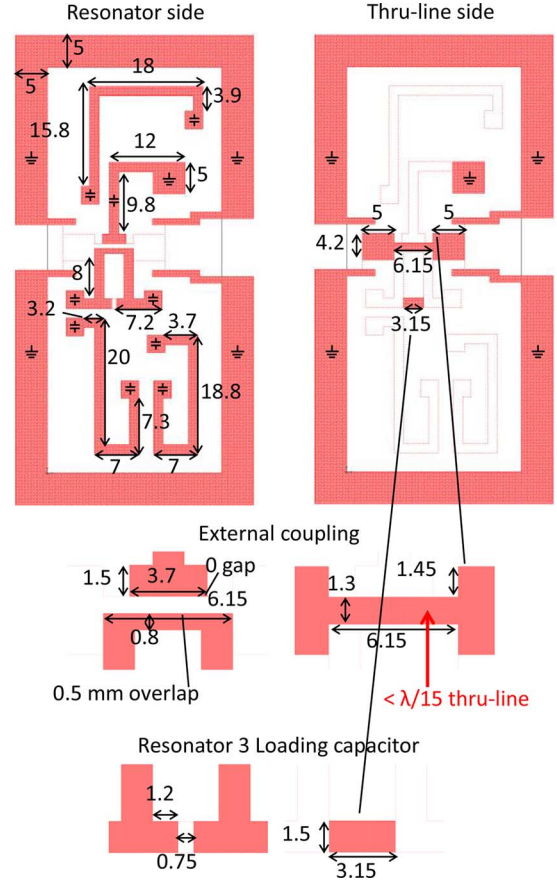


Fig. 8. Sonnet simulation layout for fifth-order suspended-stripline bandstop prototype. All dimensions are in millimeters. All resonator lines are 1.5 mm wide. All tuning capacitor pads are  $2.8 \times 2.8$  mm. Tuning capacitor locations are marked with a lumped-element capacitor symbol. Grounded pads are marked with a ground symbol.

numbered in Fig. 6(b) and are in the same configuration in Fig. 8. The half-wavelength resonators allowed the addition of pads for tuning screws on both ends of the resonators for offset tuning. Offset tuning in four of the five resonators enabled tuning of both the resonator center frequencies and coupling values between resonators after fabrication. This post-fabrication flexibility comes at a cost to the spurious-free upper passband since the next higher mode of half-wavelength resonators is at twice the fundamental frequency. In a more characterized fabrication environment, quarter-wavelength or highly loaded resonators could be used if a higher spurious-free range is desired.

Resonator 1 was designed to be a quarter-wavelength resonator due to undesired effects from coupling between higher

$$\begin{bmatrix} 0 & 0 & 0 & 0.8616 & 0 & 0 & -1.0000 & 0 \\ 0 & 0.0027 & 1.1754 & 0 & 0 & 0 & 1.6968 & 0 \\ 0 & 1.1754 & -0.0066 & 0 & 0 & 0 & 0 & 0 \\ 0.8616 & 0 & 0 & -0.0011 & 0.9435 & 0 & 0 & 0.8616 \\ 0 & 0 & 0 & 0.9435 & 0.0112 & 1.0790 & 0 & 0 \\ 0 & 0 & 0 & 0 & 1.0790 & -0.0128 & 0 & 0 \\ -1.0000 & 1.6968 & 0 & 0 & 0 & 0 & 0 & 1.0000 \\ 0 & 0 & 0 & 0.8616 & 0 & 0 & 1.0000 & 0 \end{bmatrix} \quad (14)$$

order modes that would be present if resonator 1 was implemented as a half-wavelength resonator. As can be seen in Fig. 8, resonators 1 and 3 are physically located very near to one other. Resonator 1 couples to the through-line at its electric-field maximum for the fundamental mode, and resonator 3 couples to the through-line at its magnetic-field maximum. The coupling between resonators 1 and 3 is weak at the fundamental mode due to their fields being  $90^\circ$  out of phase in the region where they are in close physical proximity. If resonator 1 was a half-wavelength resonator, its second-order mode would still couple to the through line at an electric-field maximum. Resonator 3's second-order mode couples to the through line at an electric-field maximum as well, in contrast to the fundamental-mode coupling at a magnetic-field maximum. Therefore, if resonator 1 was a half-wavelength resonator, resonators 1 and 3 would couple to each other very strongly at the second-order mode. Strong coupling causes the second-order modes to split in frequency, and one of the modes would be pushed lower into the desired upper passband of the filter. However, if resonator 1 is designed as a quarter-wavelength resonator, it does not have a mode at the frequency of resonator 3's second-order mode, and therefore resonator 3's second-order mode alone is the first spurious response in the passband. In order to increase the passband further, resonator 3 is slightly loaded with a capacitor made using the through-line side of the circuit board that can be seen in Fig. 8.

The through-line consists of two 5-mm 50- $\Omega$  lengths of line that provide an area to which the center pins of SMA connectors can be soldered. These lengths are separated by a 6.15-mm length of higher impedance line that is used to couple to resonators 1 and 3. Since the 5-mm lengths are used only for connector launching, the 6.15-mm length can be called the total functional through line, and at 3 GHz, this line has an electrical length of less than  $\lambda/15$ . A higher impedance line was used to increase coupling to resonators 1 and 3 for a given length. Since it is short with respect to the operating wavelength, the length of the higher impedance line can be matched over some bandwidth using the inductance of the step discontinuity and the capacitive loading from the resonators. The fabricated design was optimized to have the shortest possible through line with a passband that covered the S-band while not making the line so narrow that it would lead to a dominant amount of conductor loss. Note that if a passband beyond the S-band was desired, the through-line length and width could be increased slightly to reduce impedance mismatch to the ports while retaining the desired coupling values. Resonator 1 is flush (no gap or overlap) with the through line, while resonator 3 has a lateral overlap of 0.5 mm with the through line.

A model of the aluminum enclosure used to provide ground planes for the circuit can be seen in Fig. 9. The model of the top side shows the location of the nine tuning screws, which are threaded into the holes in the 1.5-mm recessed plane in the enclosure's top. Nine compression/ground screws are also present, and they are threaded through the holes in the mating faces of the two parts. Eight secure the perimeter of the clamshell enclosure, and the ninth provides grounding for one end of resonator 1.

The circuit board was fabricated using an LPKF Protolaser U3 milling machine. Photographs of the assembled circuit can

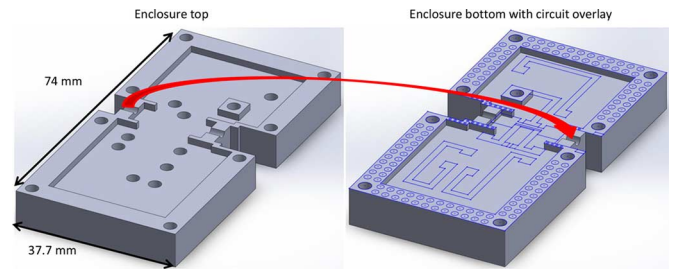


Fig. 9. Model of aluminum enclosure showing locations of tuning and compression screws. Circuit overlay is included for context. Total height of the enclosure is 17 mm.

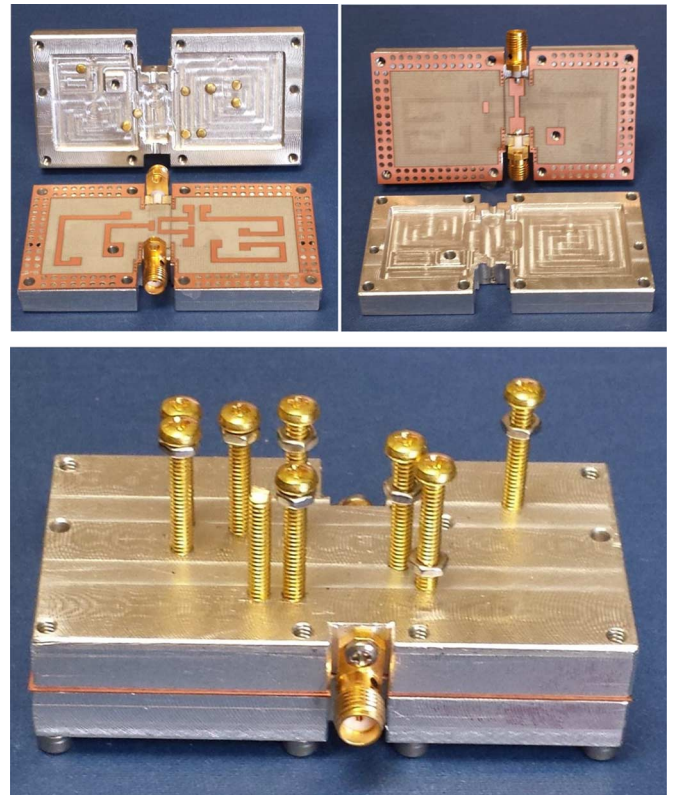


Fig. 10. Photographs of fabricated fifth-order bandstop filter.

be seen in Fig. 10. Brass 4–40-size screws were used for post-fabrication tuning, and their tips were polished so that small gaps could be achieved between the screws and the ends of the resonators. Recessed SMA connectors with an extended dielectric were used to interface with the filter while maintaining a short through line. A darkened line can be seen on both sides of the circuit board intersecting resonator 3 and traversing parallel to the through line. The line is a slightly burnt section of the circuit board that is due to its thinness and the method that the U3 laser milling machine uses to separate sectors of a layout. Finally, there are two holes in the aluminum housing that are not shown in Fig. 9, and these are tooling holes that were used during machining of the housing. They do not affect the circuit's performance.

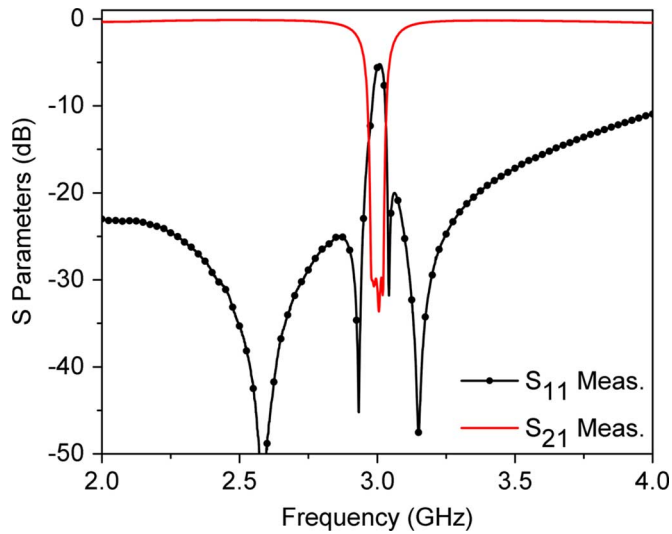


Fig. 11. S-band measured results of fabricated fifth-order bandstop filter.

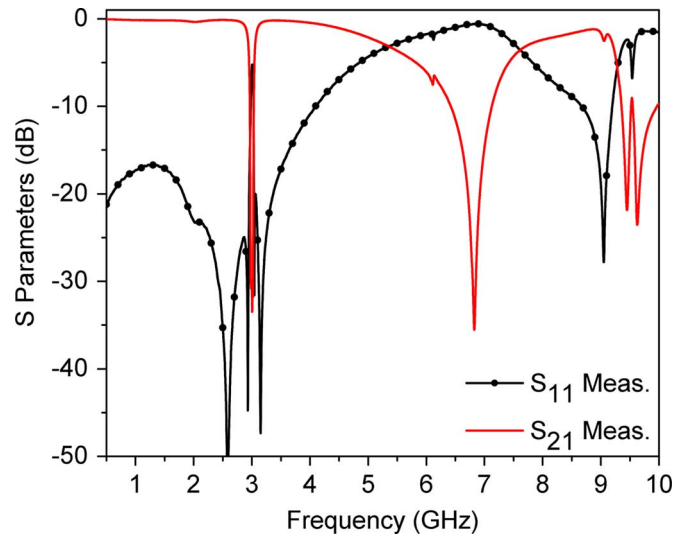


Fig. 13. Wideband measured results of fabricated fifth-order bandstop filter.

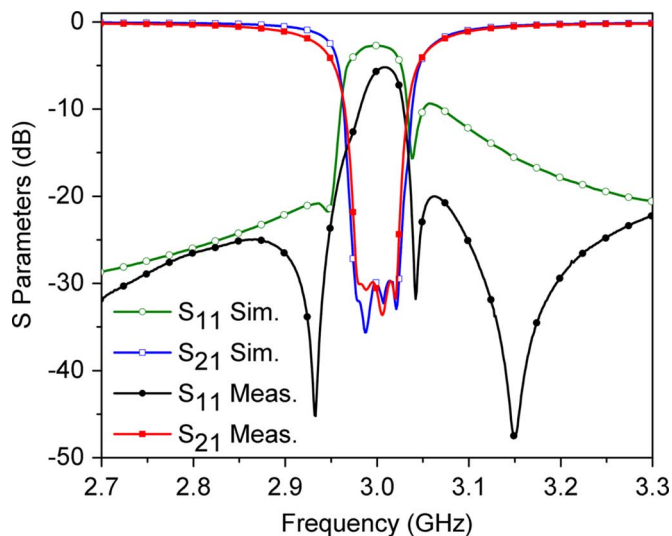


Fig. 12. Narrowband view of measured versus Sonnet-simulated results of fabricated fifth-order bandstop filter.

#### IV. MEASURED RESULTS

The fifth-order prototype was measured using an Agilent N5222A network analyzer. Due to the sensitivity of the quasi-elliptic response, first-time tuning of the circuit took approximately 1 h. However, significantly shorter tuning times were achieved for subsequent copies of the prototype. S-band measured results of the fifth-order prototype can be seen in Fig. 11. The transmission response has 30-dB equi-ripple attenuation with 42-MHz bandwidth, and the reflection response has four reflection zeros. The passband has from 0.13- to 0.45-dB attenuation across the S-band.

Narrowband measured versus simulated results can be seen in Fig. 12. The responses generally agree, but there are some notable differences. First, the resonator quality factor of the measured response is slightly lower than that of the simulated response, causing slightly narrower bandwidth for a 30-dB equi-ripple response and a more gradual passband-stopband transition. A quality factor of approximately 300 was extracted

through comparison to simulation. Reflection zero frequencies are also different due to very small differences in coupling between the resonators. Causes for such differences could include imperfect flatness of the suspended substrate, milling inaccuracies, and 3-D effects of the tuning screws. Finally, the lower frequency passband-stopband transition of the measured and simulated responses have small amounts of skewing in opposite directions. Although difficult to see in the presented tuning of the filter, there is a fifth reflection zero in the measured response near the lower frequency crossing of the transmission and reflection responses (approximately 2.97 GHz). This zero is due to an unwanted cross coupling that was not modeled. The tuning screw and port geometries were not modeled in three dimensions due to the use of 2.5-D design software.

A conventional bandstop filter was designed using the same suspended stripline environment to have the same electrical specifications as the fabricated design and simulated in Sonnet for comparison. Although the through line of the fabricated design was 15 times shorter than the conventional design, simulated passband insertion loss was approximately the same at 0.04–0.09 dB across the 2.5–3.5-GHz band. The fabricated design requires tighter coupling to the through line than a conventional design, and this causes additional passband loss per unit length.

Wideband measured results can be seen in Fig. 13. The passband starts to degrade shortly above S-band due to mismatch between the high-impedance through line and the ports. In addition, a large spurious resonance exists at approximately 6.75 GHz. This is the first spurious resonance of resonator 3, and it is slightly higher than twice the center frequency of the filter because resonator 3 is a half-wavelength resonator that is loaded with a capacitance. The small spurious resonance at approximately 6.25 GHz is due to resonator 4, which is coupled to the through line weakly due to the frequency differences between the first spurious modes of resonators 3 and 4. The first spurious resonances of resonators 1 and 2 can be seen at 9 GHz and slightly above, along with the second spurious resonance of resonator 3.

## V. CONCLUSION

The theory of reflection-mode bandstop filters with minimum through-line length was presented in this paper. Compared with both conventional and recent advanced bandstop filter topologies, the topology shown in this paper can produce bandstop responses with significantly shorter total through-line length. Functional advantages of the topology include smaller circuit volume and lower circuit weight than could be achieved with previous designs. Since many resonator types and manufacturing processes allow for both electric and magnetic field coupling, a requirement for bandstop filters with minimum through-line length, it is expected that the proposed concept could offer these advantages to many current and future bandstop filter designs.

## ACKNOWLEDGMENT

The authors would like to thank F. Wood for making mechanical drawings for the aluminum enclosure so that it could be machined.

The views, opinions, and/or findings contained in this paper are those of the authors and should not be interpreted as representing the official views or policies of the Department of Defense or the U.S. Government. Approved for Public Release, Distribution Unlimited.

## REFERENCES

- [1] L. Young, G. Matthaei, and E. Jones, "Microwave bandstop filters with narrow stop bands," in *PGMTT Nat. Symp. Dig.*, May 1962, vol. 62, no. 1, pp. 46–51.
- [2] H. Bell, "L-resonator bandstop filters," *IEEE Trans. Microw. Theory Techn.*, vol. 44, no. 12, pp. 2669–2672, Dec. 1996.
- [3] W.-H. Tu and K. Chang, "Compact second harmonic-suppressed bandstop and bandpass filters using open stubs," *IEEE Trans. Microw. Theory Techn.*, vol. 54, no. 6, pp. 2497–2502, Jun. 2006.
- [4] E. J. Naglich, J. Lee, D. Peroulis, and W. Chappell, "High-Q tunable bandstop filters with adaptable bandwidth and pole allocation," in *IEEE MTT-S Int. Microw. Symp. Dig.*, Jun. 2011, pp. 1–4.
- [5] J.-Y. Shao and Y.-S. Lin, "Millimeter-wave bandstop filter with absorptive stopband," in *IEEE MTT-S Int. Microw. Symp. Dig.*, Jun. 2014, pp. 1–4.
- [6] R. Levy, R. Snyder, and S. Shin, "Bandstop filters with extended upper passbands," *IEEE Trans. Microw. Theory Techn.*, vol. 54, no. 6, pp. 2503–2515, Jun. 2006.
- [7] R. J. Cameron, "Advanced coupling matrix synthesis techniques for microwave filters," *IEEE Trans. Microw. Theory Techn.*, vol. 51, no. 1, pp. 1–10, Jan. 2003.
- [8] S. Amari and U. Rosenberg, "Direct synthesis of a new class of bandstop filters," *IEEE Trans. Microw. Theory Techn.*, vol. 52, no. 2, pp. 607–616, Feb. 2004.

- [9] R. Cameron, Y. Wang, and M. Yu, "Direct-coupled realizations for microwave bandstop filters," in *IEEE MTT-S Int. Microw. Symp. Dig.*, Jun. 2005, 4 pp.
- [10] I. Hunter, J. Rhodes, and V. Dasonville, "Triple mode dielectric resonator hybrid reflection filters," *Proc. Inst. Electr. Eng.—Microw., Antennas, Propag.*, vol. 145, no. 4, pp. 337–343, Aug. 1998.
- [11] P. Phudpong and I. Hunter, "Frequency-selective limiters using nonlinear bandstop filters," *IEEE Trans. Microw. Theory Techn.*, vol. 57, no. 1, pp. 157–164, Jan. 2009.
- [12] J. Rhodes and I. Hunter, "Synthesis of reflection-mode prototype networks with dissipative circuit elements," *IEE Proc. Inst. Electr. Eng.—Microw., Antennas, Propag.*, vol. 144, no. 6, pp. 437–442, Dec. 1997.
- [13] R. Gomez-Garcia, J. Alonso, and D. Amor-Martin, "Using the branch-line directional coupler in the design of microwave bandpass filters," *IEEE Trans. Microw. Theory Techn.*, vol. 53, no. 10, pp. 3221–3229, Oct. 2005.
- [14] W. Fathelbab, "Synthesis of cul-de-sac filter networks utilizing hybrid couplers," *IEEE Microw. Wireless Compon. Lett.*, vol. 17, no. 5, pp. 334–336, May 2007.
- [15] D. R. Jachowski, "Synthesis of lossy reflection-mode bandstop filters," in *Int. Microw. Filters Workshop*, Oct. 2006, pp. 1–40.
- [16] E. J. Naglich and A. C. Guyette, "Bandstop filters with minimum through-line length," in *IEEE MTT-S Int. Microw. Symp. Dig.*, May 2015, pp. 1–4.
- [17] A. Guyette, "Intrinsically switched varactor-tuned filters and filter banks," *IEEE Trans. Microw. Theory Techn.*, vol. 60, no. 4, pp. 1044–1056, Apr. 2012.
- [18] D. M. Pozar, *Microwave Engineering*, 3rd ed. New York, NY, USA: Wiley, 2005, pp. 412–416.
- [19] H. Bell, "The coupling matrix in low-pass prototype filters," *IEEE Microw. Mag.*, vol. 8, no. 2, pp. 70–76, Apr. 2007.



**Eric J. Naglich** (S'09–M'14) received the B.S. and Ph.D. degrees in electrical and computer engineering from Purdue University, West Lafayette, IN, USA, in 2007 and 2013, respectively.

From 2007 to 2009, he was with GE Healthcare, where he was involved with the Edison Engineering Development Program. In February 2014, he joined the U.S. Naval Research Laboratory (NRL), Washington, DC, USA, where his current research is focused on reconfigurable filter and passive circuit synthesis and fabrication techniques.

Dr. Naglich is a 2013 Karle Fellow. He was a National Defense Science and Engineering Graduate (NDSEG) Fellow.



**Andrew C. Guyette** (M'08–SM'15) was born in Grand Forks, ND, USA, in 1976. He received the B.S. and M.S. degrees in electrical engineering from the University of Hawaii at Mānoa, Honolulu, HI, USA, in 1999 and 2001, respectively, and the Ph.D. degree from The University of Leeds, Leeds, U.K., in 2006.

Since 2007, he has been with the U.S. Naval Research Laboratory, Washington, DC, USA. His research interests include tunable filters, lossy filters, and network synthesis.